Estimation of Daily Actual Evapotranspiration Using Vegetation Coefficient Method for Clear and Cloudy Sky Conditions

Hassan Rangaswamy Shwetha and Dasika Nagesh Kumar

***Abstract*—Actual evapotranspiration (AET) can be studied and estimated using remote-sensing-based methods at multiple spatial and temporal scales. Reflectance and Land surface temperature are essential in these methods. However optical and thermal sensors fail to provide these data under overcast conditions and this creates gap in the AET product. Besides, there is a necessity of the AET method that requires less data and estimates AET with better accuracy. In this regard, AET was estimated for all-sky conditions using the vegetation coefficient (VI-Kv) method utilizing microwave, thermal, and optical data. Essential reference evapotranspiration (ET_0) under cloudy conditions was estimated using LST-based Penman–Monteith temperature (PMT) and Hargreaves–Samani equations. Furthermore, LST predicted using the microwave polarization difference index (PLST) and LST of moderate resolution imaging spectroradiometer (MODIS) cloud product (MLST) were evaluated with in-situ air temperature (Ta) under cloudy sky conditions. Results revealed that the PLST correlated better with Ta than MLST with correlation coefficient (*r*) values of 0.71 and 0.81 for day and night times, respectively. Hence, PLST-based solar radiation (Rs) estimation yielded better accuracy with observed Rs with *r* and root mean square error values of 0.864 and 0.07 for Berambadi station under cloudy conditions, respectively. PMT-based ET_0 values corresponded well with the observed ET_0 under cloudy sky condition during this study. In addition, AET estimated using the VI-Kv method was compared with the simple two-source energy balance (TSEB) method under clear sky conditions. It was found that the improved VI-Kv method performed better than the TSEB method and could also fairly estimate AET even under cloudy sky conditions.**

***Index Terms*—Cloudy sky, daily actual evapotranspiration, vegetation coefficient.**

I. Introduction

Water scarcity is a major problem facing a number of nations in the present time. This is attributed to increased demand for freshwater by the competing users in different sectors and, more importantly, leads to environmentally induced problems, such as desertification and overexploitation of the existing water resources. Dependence on rainfall for future crop production has become a major constraint for sustainable food production in developing countries. Irrigated agriculture accounts for about 70% usage of the available freshwater globally [1]. In many areas of the world, where rainfall is too low or insufficient to meet the water demand of the crops, irrigation is a significant component of agricultural (cropping pattern) planning. In irrigated/rain-fed agriculture, it is necessary to establish when and how much water to supply and, of course, to determine the optimum sowing time to take advantage of the available soil moisture and precipitation. Irrigation water demand is usually determined through evapotranspiration (ET) estimation procedures. Apart from precipitation, ET is the most significant component of the hydrological budget. Actual ET (AET) is measured using ground-based measurements, such as lysimeters, eddy covariance, and Bowen ratio at point scale with high temporal resolution. These are difficult to be extended to obtain the spatial distribution of AET at the basin scale, and also these involve high installation and maintenance costs. In this regard, satellite images provide required data for the estimation of the spatial distribution of AET at fine spatial resolution using satellite-based physical, empirical, and semiempirical models at the basin or regional to global scales.

The important satellite-based models for the estimation of AET are energy balance (EB), vegetation-coefficient-based (VI-Kv), and contextual-based methods. EB method consists of one (OSEB) or two-source EB (TSEB) models, and these have been applied in many regions [2]– [14]. A few researchers compared these EB methods and found that the TSEB models performed well for a particular study region [15]– [17]. TSEB models are more effective than OSEB models as these calculate AET for soil and vegetation surfaces separately. Therefore, in this study, the TSEB model was considered to estimate AET under clear sky conditions and compared with AET estimated using the improved VI-Kv method. Many researchers have applied the VI-Kv method and obtained good results for their respective study regions [18]–[23]. Furthermore, this method has the advantage to obviate temporal upscaling from instantaneous to daily scale. Few studies have compared EB models with the VI-Kv method. Gonzalez-Dugo *et al.* [24] compared EB

Manuscript received April 10, 2019; revised November 15, 2019 and February 25, 2020; accepted April 9, 2020. Date of publication May 14, 2020; date of current version June 1, 2020. This work was supported by the Ministry of Earth Sciences, Government of India, through a project under Reference Number MoES/PAMC/ H&C/41/2013-PC-II. *(Corresponding author: Dasika Nagesh Kumar.)*

Hassan Rangaswamy Shwetha was with the Interdisciplinary Centre for Water Research, Indian Institute of Science, Bengaluru 560012, India. She is now with the Department of Applied Mechanics and Hydraulics, National Institute of Technology, Surathkal, Mangalore 575025, India (e-mail: hrshwetha@nitk.edu.in).

Dasika Nagesh Kumar is with the Department of Civil Engineering, Indian Institute of Science, Bengaluru 560012, India (e-mail: nagesh@iisc.ac.in).

Digital Object Identifier 10.1109/JSTARS.2020.2989422

models and reflectance-based VI-Kv model over rainfed corn and soybean crops in central lowa. AET was estimated using the procedures of TSEB models developed by Norman *et al.* [25], [26]. The VI-Kv method uses FAO methodology based on the concepts of vegetation coefficient (Kv) and reference ET (ET_0). They found that TSEB performed slightly better than other models because thermal-based EB models could inherently account for AET reduction due to plant water stress. Consoli and Vanella [27] performed comparative analysis between EB models and reflectance-based VI-Kv method for a Mediterranean semiarid environment. AET was estimated using TSEB and VI-Kv models in the same manner as given by Gonzalez-Dugo *et al.* [24]. In this case also, the TSEB model yielded better performance than other models.

EB and VI-Kv models require data such as land surface temperature (LST) and vegetation indices obtained from measurements of thermal and optical regions of the electromagnetic radiation. But these are affected by the presence of clouds and fail to provide data, resulting in discontinuity in the AET product. EB algorithms cannot be applicable under cloudy conditions since the unavailability of required satellite data under cloudy sky conditions. These algorithms are data intensive and time-consuming compared with the VI-Kv method. Some of the EB algorithms require ground-based measurements to obtain AET [28]. Variations in evaporative fraction (EF) are controlled by the presence of clouds and aerosols to a larger extent. Hence, EF-based AET estimation is very difficult to be employed under cloudy sky conditions [29], whereas the VI-Kv method can be applicable even under cloudy sky conditions [30], [31]. Satellite-based latent heat flux must be temporally upscaled to longer time frames to be useful to hydrology, over which clouds will influence the surface EB (for e.g., monthly time steps over years) [32]. But even the application of reconstruction models to obtain continuous AET, using AET values obtained under clear sky conditions, these values overestimate AET to account for longer time frames. This motivates the estimation of AET for all-sky conditions using the VI-Kv method. Very few researchers have estimated AET under cloudy conditions. Kim and Hogue [33] evaluated moderate resolution imaging spectroradiometer (MODIS)-based daily potential ET estimated using the Priestly–Taylor equation for all-sky conditions at point scale. Ruan *et al.* [34] evaluated EF constant and solar-radiation-based AET algorithms to convert instantaneous measurements to daily ET for all-sky conditions, and results revealed that both algorithms yielded large errors for cloudy conditions during the growing season. Luo *et al.* [28] estimated ET for all-sky conditions using an extension of the Priestly–Taylor model with contextual interpretation of remotely sensed LST and vegetation index utilizing MODIS cloud product. It is necessary to utilize microwave data because usually 50% of the earth surface is covered by the cloud at any time [35]. Recently, few researchers have combined microwave and optical sensor observations to improve the accuracy of AET under cloudy sky conditions [36]–[38]. Sun *et al.* [36] utilized microwave soil moisture and thermal remote sensing in TSEB over southern great plains using a simple model and a stationary-based method for parameter estimation and suggested that microwave and thermal remote sensing together could improve the energy and water fluxes, but the produced AET was at coarser resolution. Bastiaanssen *et al.* [37] proposed the ETlook remote sensing model employing combined microwave and optical sensor observations in the two-layer Penman–Monteith (PM) equation. Leng *et al.* [38] estimated AET using the trapezoidal two-stage LST/fractional vegetation cover feature space method under clear sky conditions, and the PM equation with meteorological data over cloudy sky pixels. However, in these studies, meteorological data are required, which are difficult to be obtained, especially in remote areas. In addition, microwave-based soil moisture needs further improvement to be utilized in these models [37], [39]. Therefore, there is a necessity of a simple method that estimates accurate AET for all-sky conditions at high spatio-temporal resolution with less dataset obtained from satellites.

The overall intent of this study was to estimate AET for all-sky conditions using a simple method with less dataset. To achieve this, the following objectives were set for the study.

1) Evaluation of LST products to be utilized in ET_0 models under overcast conditions.
2) Comparison of AET estimated using TSEB and VI-Kv methods under clear sky conditions.
3) Estimation of ET_0 and AET using the VI-Kv method under cloudy conditions.

In this context, the VI-Kv method was selected as it can be applied under all-sky conditions. Required LST under cloudy sky conditions was predicted using the microwave polarization difference index (MPDI) with ancillary data and artificial neural networks (ANN) [40]. Improved Kv values, which account for transpiration from vegetation and evaporation from the soil, were employed in the VI-Kv model to estimate AET. It was found that the combination of the global vegetation moisture index (GVMI) and temperature vegetation difference index (TVDI) could better represent Kv values than other vegetation indices for clear pixels [41]. The spatial distribution of ET_0 was estimated from temperature-based PM temperature (PMT) and Hargreaves–Samani (HS) equations using only LST over cloudy and air temperature (Ta) over clear sky pixels [42]. Moreover, in this study, LST predicted from MPDI and MODIS LST from cloud products were evaluated with Ta measurements from AWS to estimate ET_0 under cloudy conditions. Derived continuous Kv using the regression technique [41] was used with ET_0 to estimate AET under cloudy sky conditions.

II. Study Area and Data Used

The Cauvery River is one of the major rivers of peninsular India, and the river basin extends between 10°05′–13°30′N and 75°30′–79°45′E. The River basin covers an area of 81 155 km^2 and lies in the states of Karnataka, Kerala, Tamil Nadu, and Pondicherry. It is one of the largest rivers of southern India and depends heavily on monsoon rains; hence, it is prone to droughts when the monsoon fails. In terms of physiography, the basin can be divided into three parts: the Western Ghats area, the Plateau of Mysore, and the Delta area [43]. The Delta forms the lower part of the Cauvery basin and is the most fertile tract, whereas the Western Ghats consists of a mountainous region and runs parallel

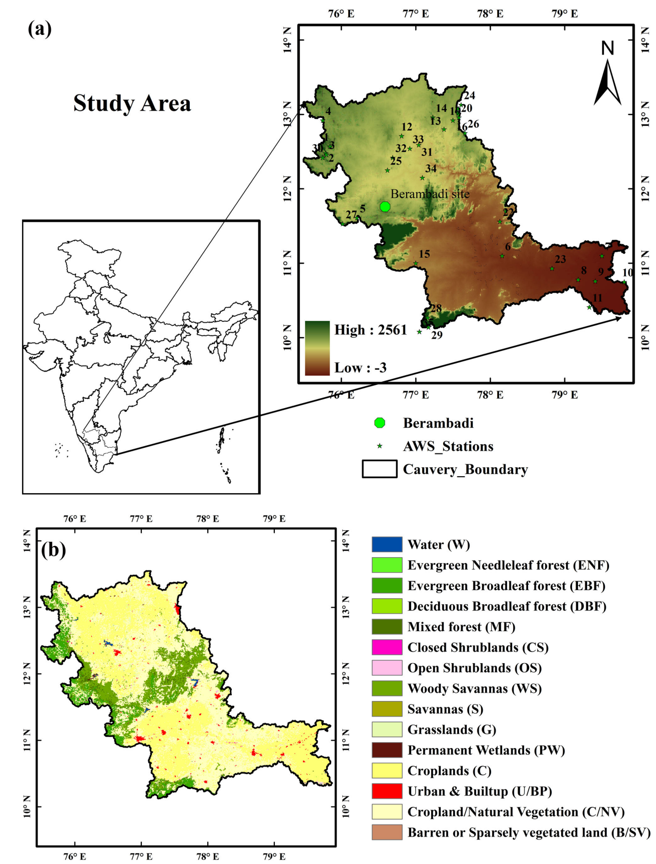

Fig. 1. (a) Location of the study area with the AWS indicated by numbers. Station IDs 1–5 belong to forest (F), station IDs 6–14 belong to croplands (C), station IDs 15–18 belong to urban/builtup (U/BP), and stations IDs 19–35 belong to croplands/natural vegetation (C/NV) land cover classes, location of the Berambadi station is indicated in green circle and also elevation of the study area is depicted. (b) MODIS land use land cover map of the study area.

to the western coast [see Fig. 1(a)]. The mean maximum ($T_{\max}$) and minimum ($T_{\min}$) air temperatures are 34.30 °C and 17.15 °C, respectively, for the period 1969–2004.[1] Precipitation varies substantially over the basin, whereas the western part of the basin receives the southwest monsoon (June–September), and the northeast monsoon (October–December) serves the eastern part. The rainfall during other periods is insignificant. The basin receives a mean annual precipitation of about 1075 mm/year. Annual rainfall (1970–2004) varies from 1700 to 3800 mm/year in the Western Ghats and from 600 to 800 mm/year in the Plateau of Mysore, whereas the Delta area receives 500–1000 mm/year (www.india-wris.nrsc.gov.in). Land use/land cover of the basin is broadly classified as agricultural, nonagricultural, forest, and habitation land. Data for the year 2012 show more than 60% of the land in the Cauvery basin is cultivable, 1.15% is urban/built-up, 17.91% is forest regions, and the remainder is noncultivable. Finger millet and paddy are the principal crops of the Mysore Plateau and Delta regions, respectively.

MODIS reflectance values (MYDO9GA) of RED, NIR, BLUE, SWIR1 bands, Albedo (MCD43B3), leaf area index (LAI), sun elevation angle, emissivity, and LST (MYD11A1) were available at 500 m and 1 km resolutions, respectively, in sinusoidal projection. These were converted to geographical projection systems by the nearest neighbor method using MODIS reprojection tool developed by NASA [44]. MODIS LULC (MCD12Q1) and SRTM elevation were also upscaled from 500 m and 90 m to 1 km respectively. All these data were used in the TSEB model to estimate AET under clear sky conditions. Brightness temperature (T_b) at 36.5 GHz channel of Advanced Microwave Scanning Radiometer (AMSR-2) was utilized to predict LST under cloudy sky conditions [38]. Meteorological data such as $T_{\max}$, $T_{\min}$, relative humidity, wind speed, and sunshine hours required for the estimation of ET_0 using the FAO56-PM method were acquired from the automatic weather stations (AWS) installed by the Indian Space Research Organization (ISRO). A total of 35 AWSs located within the basin were considered in this study, and these were used to evaluate LST products. In situ latent heat flux (LE, W/m^2) and weather variables such as Ta, relative humidity, air pressure, wind speed and direction, solar radiation (Rs) were collected from the Berambadi station for the year 2013, which is located in the middle of croplands near Lakkipura village in Gundalpet taluk of Karnataka state (11.76°N; 76.58°E) and altitude of 870 m (see Fig. 1). LE was estimated using the Bowen ratio EB equation using data from the 10-m-tall micrometeorological tower (popularly called Agro-Met station and abbreviated as AMS established by ISRO at the site [45]. LE was converted into AET (mm/day) and used for validation of the estimated AET using satellite data for all-sky conditions. Weather variables obtained from the AMS are used to estimate ET_0 using the FAO56-PM equation, which was used to validate ET_0 estimated using remote- sensing-based temperature-based models and vegetation coefficients for all-sky conditions. Details about the data used are provided in Table I.

III. Methodology

A. *Comparison of LST Products Under Cloudy Sky Conditions*

LST is a very important variable to estimate ET_0 under cloudy conditions; hence, the evaluation of available LST products is essential. In literature, Ta was estimated using MODIS cloud LST (MYDO6_L2) product to obtain net radiation under cloudy sky conditions [46], [28]. Shwetha and Nagesh [40] predicted LST using an MPDI with ancillary data. In this study, these two LST products were evaluated with measured Ta at AWS locations. Hereafter predicted LST using MPDI with ancillary data and MODIS cloud LST during the day and night times were referred to as PLST (day/night) and MLST (day/night), respectively, under cloudy sky conditions. MPDI and PLST can be derived as

$$\mathrm{MPDI}_s = \frac{T_{bv} - T_{bh}}{0.5 * \ (T_{bv} + T_{bh})} \tag{1}$$

$$\mathrm{PLST}^{1\mathrm{km}}\,(\mathrm{day/night}) = f\left(\begin{array}{c}\mathrm{MPDI}_s^{1\mathrm{km}}\,(\mathrm{day/night})\,, \\ \mathrm{elevation, latitude, longitude, Julian\ day}\end{array}\right) \tag{2}$$

where T_{bv} and T_{bh} denote brightness temperature at vertical (v) and horizontal (h) polarizations, respectively, and the subscript

[1]Online. [Available]: http://www.india-wris.nrsc.gov.in

TABLE I
DETAILS OF THE DATASET USED IN THIS STUDY

Source	Parameter	Product Name	Spatial Resolution	Purpose
MODIS/Aqua	LST(day/night), emissivity	MYD11A1	1 km	TSEB model and to estimate Kv
MODIS/Aqua	Reflectance values of NIR, Red, Blue and SWIR2 bands	MYD09GA	500 m	TSEB model and to estimate Kv
MODIS/Aqua	LULC	MCD12Q1	500 m	Segregation of Kv and LST
MODIS/Aqua	Albedo, LAI, sun elevation angle	-	1 km	TSEB model
AMSR-2/Aqua	Tb at 36.5 GHz	-	25 km	To predict LST
SRTM	Elevation	-	90 m	TSEB model and to predict LST, Ta
AWS	RH (max/min), Ta (max/min), wind speed and sunshine hour	-	Point scale	Validation
Berambadi Station	RH (max/min), Ta (max/min), wind speed and sunshine hour and latent heat flux	-	Point scale	Validation

Note. LST = land surface temperature, LULC = land use land cover, LAI = leaf area index, Tb = brightness temperature, RH = relative humidity, Ta = air temperature, TSEB = two-source energy balance, Kv = vegetation coefficient.

"s" indicates AMSR2 sensor derived product. The best LST (day/night) product was used instead of air temperature extremes in PMT and HS ET_0 models since the difference between LST and Ta under cloudy sky conditions is less [47], [48].

B. Estimation of AET for Clear and Cloudy Sky Conditions

Estimation of AET was carried out using the TSEB model under clear sky conditions and the VI-Kv method for all-sky conditions. Clear and cloudy pixels were classified depending on the availability of MODIS LST data at a 1-km spatial resolution. If the LST value is present for the pixel, it is considered as a clear pixel or else as a cloudy pixel. The improved VI-Kv method has been compared with the TSEB model in order to check its performance by evaluating AET values with the observed AET values at Berambadi station under clear sky conditions.. The schematic representation of the estimation of AET for all-sky conditions is shown in Fig. 2.

1) Two-Source Energy Balance Model: EF expressed as the ratio of AET to the available energy was estimated separately as a mixture of EF of bare soil and EF of vegetation as proposed by Nishida *et al.* [49]. By assuming negligible coupled energy transfer between vegetation and bare soil for a pixel, AET can be expressed as a linear combination of AET from vegetation ($\mathrm{ET_{veg}}$) and AET from bare soil ($\mathrm{ET_{soil}}$), and it can be expressed as

$$\mathrm{AET} = f_{\mathrm{veg}}\mathrm{ET}_{\mathrm{veg}} + (1 - f_{\mathrm{veg}})\,\mathrm{ET}_{\mathrm{soil}} \tag{3}$$

$$f_{\mathrm{veg}} = \frac{\mathrm{NDVI} - \mathrm{NDVI}_{\mathrm{min}}}{\mathrm{NDVI}_{\mathrm{max}} - \mathrm{NDVI}_{\mathrm{min}}} \tag{4}$$

where f_{veg} is a fraction of vegetation, NDVI is normalized difference vegetation index, $\mathrm{NDVI}_{\mathrm{min}}$ and $\mathrm{NDVI}_{\mathrm{max}}$ are minimum and maximum NDVI of bare soil and full vegetation, respectively. $\mathrm{ET_{veg}}$ and $\mathrm{ET_{soil}}$ can be expressed in terms of EF. These are given as

$$\mathrm{ET}_{\mathrm{veg}} = Q_{\mathrm{veg}}\mathrm{EF}_{\mathrm{veg}} \tag{5}$$

$$\mathrm{ET}_{\mathrm{soil}} = Q_{\mathrm{soil}}\mathrm{EF}_{\mathrm{soil}} \tag{6}$$

$$Q_{\mathrm{veg}} = R_n. \tag{7}$$

The difference between available energy for vegetation (Q_{veg}) and available energy for soil (Q_{soil}) is due to the differences in thermal emission, solar reflectance, and ground heat flux between bare soil and vegetation [49]. R_n is net radiation. $\mathrm{EF_{veg}}$ can be calculated using complementary relationship based on advection aridity by converting $\mathrm{ET_{veg}/PET_{veg}}$ to $\mathrm{EF_{veg}}$, and it is given as

$$\mathrm{EF}_{\mathrm{veg}} = \frac{\alpha\Delta}{\Delta + \gamma\,(1 + r_c/2r_a)} \tag{8}$$

where α is the Priestly–Taylor parameter, Δ is derivative of saturated vapor pressure (Pa/K), γ is psychrometric constant (Pa/K), r_c is surface resistance of vegetation canopy, r_a is aerodynamic resistance. $\mathrm{EF_{soil}}$ was estimated by considering the energy budget of bare soil

$$\mathrm{EF}_{\mathrm{soil}} = \frac{T_{\mathrm{soil\ max}} - T_{\mathrm{soil}}}{T_{\mathrm{soil\ max}} - \mathrm{Ta}}\left(\frac{Q_{\mathrm{soil}\,0}}{Q_{\mathrm{soil}}}\right) \tag{9}$$

where $T_{\mathrm{soil\,max}}$ and T_{soil} are maximum and actual bare soil temperatures, respectively, Ta is air temperature. Q_{soil0} is available energy when T_{soil} is equal to Ta. T_{soilmax} and T_{soil} can be estimated using the vegetation index-LST (VI-LST) diagram. Q_{soil} is calculated using an energy budget, which is given as

$$Q_{\mathrm{soil}} = (1 - C_G)\left[R_{n0} - 4\varepsilon\sigma\mathrm{Ta}^3\,(T_{\mathrm{soil}} - \mathrm{Ta})\right] \tag{10}$$

where C_G is an empirical coefficient ranging from 0.3 for wet soil to 0.5 for dry soil[49]. R_{n0} is net radiation if T_{soil} is equal to Ta. ε is the emissivity, and σ is the Stefan–Boltzmann constant.

2) Vegetation Coefficient Method: Daily AET can be estimated using the VI-Kv method for all-sky conditions and 11). In this study, improved Kv values were employed with ET_0 values to estimate AET for the study region

$$\mathrm{AET} = \mathrm{ET}_0 * \mathrm{Kv}. \tag{11}$$

For this purpose, ET_0 was calculated from the PMT method using only Ta as input for clear sky conditions. Kv was estimated using a combination of GVMI and TVDI, where GVMI represents the transpiration coefficient from plants, and TVDI represents the evaporation coefficient from the soil. More details on the estimation of Kv are provided in [41]. MODIS LST with ancillary data was used to estimate Ta (max/min) values using the advanced statistical approach, as given in (13) and (14) [42]. These were employed in ET_0 estimation under clear sky conditions using PMT [see (12)]. The crucial inputs required in the VI-Kv method, such as LST and reflectance values, were collected from MODIS sensor for clear sky conditions. The main disadvantage of MODIS sensor is that it fails to produce these data under cloudy sky conditions. Therefore, LST (day/night) values were predicted under cloudy sky conditions using microwave measurements and ANN models using (2) [40]. These

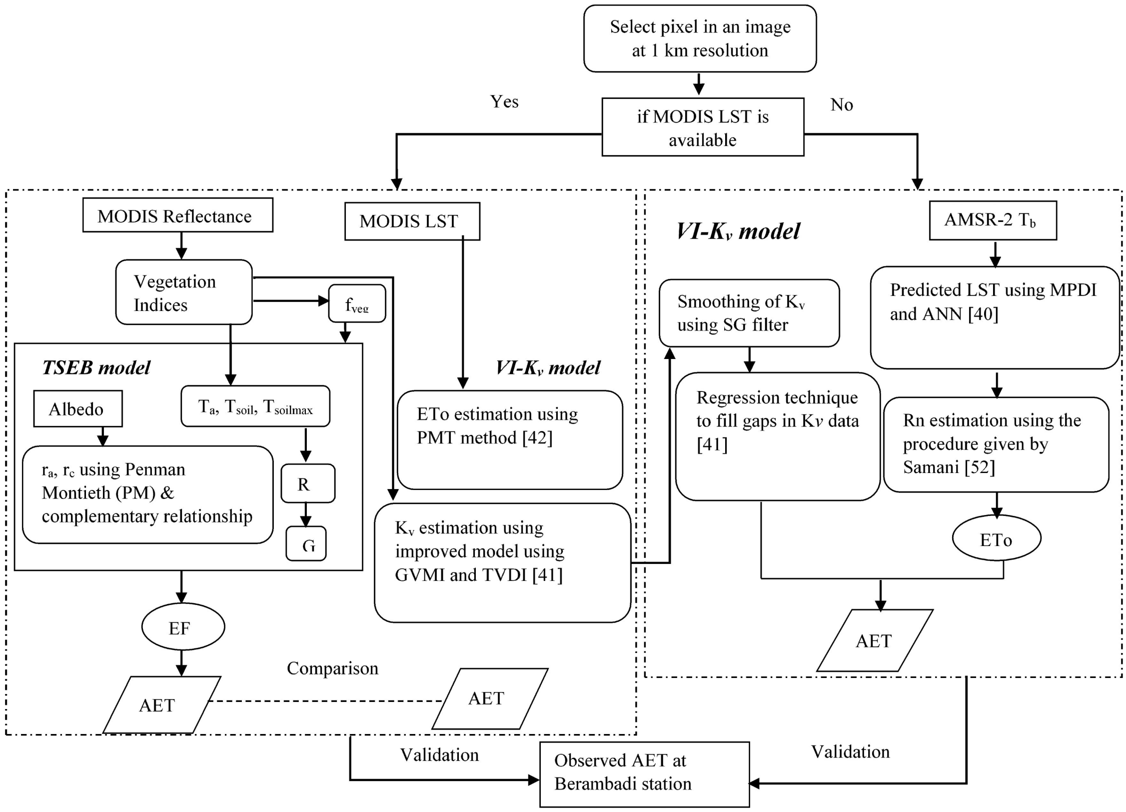

Fig. 2. Schematic representation of methodology.

LST (day/night) values were employed separately in PMT and HS equations to estimate ET_0 since the difference between LST and Ta under cloudy sky conditions is less [47], [48] and also to evaluate the applicability of the LST data in both PMT and HS equations.

Estimation of ET_0 using PMT for all-sky conditions uses a procedure given by Todorovic *et al.* [50]. This procedure consists of estimating required inputs of the PMT equation using only temperature (LST or Ta)

$$\mathrm{ET}_0 = \frac{0.408\Delta\,(\mathrm{Rn} - G) + \gamma\left(\frac{900}{\mathrm{Ta}+237}\right) u_2\,(e_s - e_a)}{\Delta + \gamma\,(1 + 0.34u_2)}. \quad (12)$$

Here, Ta is the mean daily air temperature (°C) at 2 m, u_2 is the average daily wind speed (m/s) at 2 m, Rn is the net daily radiation ($\mathrm{MJm^{-}day^{-1}}$), G is the soil heat flux ($\mathrm{MJm^{-2}day^{-1}}$), $e_s - e_a$ is the vapor pressure deficit (kPa), γ is the psychometric constant (kPa $°\mathrm{C}^{-1}$), and γ is the slope of the saturation vapor pressure curve (kPa $°\mathrm{C}^{-1}$). Ta (max/min) were calculated under clear sky conditions using the advanced statistical approach from (13) and (14)

$$T_{\max} = a * \mathrm{LST_{day}} + b * \mathrm{LST_{night}} + c* \times \left(\cos\left(\pi * \left(\frac{\mathrm{jday + peak}}{\mathrm{phase}}\right)\right)\right) + d * \mathrm{ele} + e \quad (13)$$

$$T_{\min} = a * \mathrm{LST_{day}} + b * \mathrm{LST_{night}} + c \quad (14)$$

where $T_{\max}$ and $T_{\min}$ are maximum and minimum air temperatures, respectively. $\mathrm{LST_{day}}$ and $\mathrm{LST_{night}}$ are daytime and nighttime LSTs, respectively, peak and phase are coefficients of the cosine function, letters *a* to *e* are coefficients of models, jday is Julian day, and ele is elevation. Daily net radiation (Rn) was estimated using the procedure proposed by Samani [50], [51]

$$\mathrm{Rn} = R_{\mathrm{ns}} + R_{nl} \quad (15)$$

$$R_{ns} = (1 - \alpha)\,\mathrm{Rs} \quad (16)$$

where R_{ns} and Rs are net shortwave radiation ($\mathrm{MJ/m^2/day}$) and daily shortwave radiation ($\mathrm{MJ/m^2/day}$), respectively. α is the albedo, and it is fixed as 0.23 for grass reference crop. Rs can be calculated as

$$\mathrm{Rs} = k_{rs}\sqrt{(T_{\max} - T_{\min})}\mathrm{Ra} \quad (17)$$

$$\mathrm{Rs/Ra} = k_{rs}\sqrt{(T_{\max} - T_{\min})} \quad (18)$$

where Rs/Ra is a clearness index, which accounts for the effect of cloudiness and humidity at a location [52], and it ranges from more than 0.75 on clear sky day to 0.25 on a day with dense clouds. Ra is extraterrestrial radiation in mm/day and can be calculated using the procedure given in [53]. k_{rs} is empirical coefficient that was initially adopted as 0.17 for semiarid regions but later Hargreaves [54] recommended 0.162 for interior regions and 0.19 for coastal regions. However, the k_{rs} differs from region to region; hence, it is necessary to correct for its variations. In this study, the procedure suggested by Allen [53] was followed to calculate k_{rs} for the study region

$$K_T = k_{rs}\sqrt{(P/P_O)} \tag{19}$$

k_{rs} is 0.162 for interior regions and 0.19 for coastal regions. *P* is the mean atmospheric pressure, which can be estimated by

$$P = \{P_O\,(293 - [(0.0065 * Z)/293])\}^{5.26} \tag{20}$$

where P_o is the mean atmospheric pressure at sea level (101.3 kPa). *Z* is the elevation in meter. R_{nl} under cloudy sky can be calculated as

$$R_{nl} = fR_{bo} \tag{21}$$

$$R_{bo} = -\bar{\varepsilon}\sigma\left(\frac{T^4_{\max} + T^4_{\min}}{2}\right) \tag{22}$$

$$f = a_c\left(\frac{\mathrm{Rs}}{R_{\mathrm{so}}}\right) + b_c \tag{23}$$

where *f* is the cloudiness factor, R_{bo} is net longwave radiation under clear skies. ε is the net emissivity $T_{\max}$ and $T_{\min}$ are maximum and minimum air temperatures, respectively in Kelvin. $\mathrm{Rs}/R_{\mathrm{so}}$ is relative solar radiation, where R_{so} is the maximum possible solar radiation in the absence of cloud cover and provides an estimate of the degree of cloudiness in the atmosphere, and this ratio generally varies between 0.33 (dense cloud cover) and 1 (clear sky). The coefficients $a_c = 1.35$ and $b_c = -0.35$ are recommended by Smith *et al.* [55]. R_{so} is calculated as

$$R_{\mathrm{so}} = (0.75 + 2 * 10^{-5}Z)R_a \tag{24}$$

where *Z* is elevation. ET_0 is also estimated using the HS equation, which is given as

$$\mathrm{ET}_0 = 0.408 * c_H * R_a * (T_{\mathrm{mean}} + 17.8) * \sqrt{T_{\mathrm{diff}}}. \tag{25}$$

Here, T_{mean} is mean temperature (°C), T_{diff} is the difference between maximum and minimum air temperature (°C). c_H is Hargreaves empirical coefficient set to 0.0023 for arid and semiarid regions. Kv values for all-sky conditions were estimated using the regression technique [41]. These were multiplied with ET_0 values to obtain AET.

IV. Results and Discussion

A. Comparison of LST Products Under Cloudy Sky Conditions

In this study, PLST (day/night) and MLST (day/night) were evaluated with corresponding in situ $T_{\max/\min}$ (O) measurements from AWS. PLST was found to be more accurate than MLST with correlation coefficient (*r*) values of 0.71 and 0.82 for day and night times, respectively (see Fig. 3). Therefore, in this study, $\mathrm{PLST}_{\max/\min}$ was used to estimate ET_0 under cloudy sky conditions for the study region. Furthermore, separate analyses were carried out for different seasons; red, blue, green, and yellow colors in Fig. 3 indicate winter, monsoon, postmonsoon, and summer seasons, respectively. However, in winter and rainy seasons, $\mathrm{PLST}_{\max/\min}$ values agrees better with the corresponding $T_{\max/\min}(\mathrm{O})$ measurements when compared with postmonsoon and summer seasons.

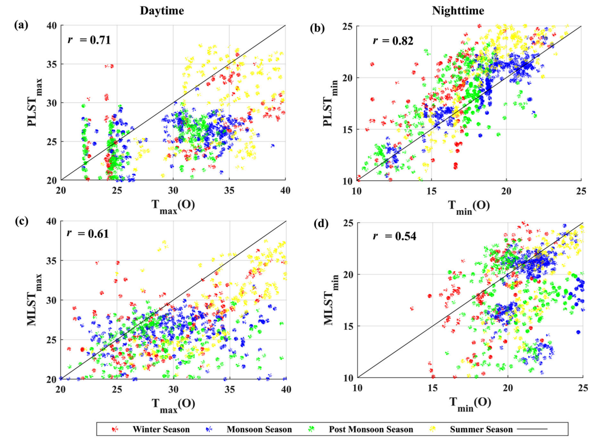

Fig. 3. Comparison of (a) and (b) PLST and (c) and (d) MLST products with Ta obtained from AWS locations during day and night times.

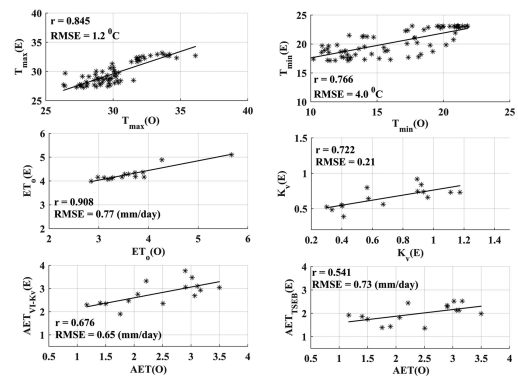

Fig. 4. Scatter plots between satellite-based $T_{\max}$, $T_{\min}$, ET_0, Kv, and AET estimated using the VI-Kv method ($\mathrm{AET}_{\mathrm{VI-Kv}}$) and TSEB method ($\mathrm{AET}_{\mathrm{TSEB}}$) and corresponding observed values at Berambadi station for clear pixels.

B. Comparison of AET Values Estimated Using the Kv Model and the TSEB Model With Observed AET Under Clear Sky Conditions

Latent heat flux is obtained using the Bowen ratio method at Berambadi station for the year 2013 and later was converted to AET. This was used to evaluate estimated AETs using TSEB and the VI-Kv methods. Fig. 4 depicts the relationship between estimated AET using the VI-Kv and TSEB methods and observed AET values. In addition to this, inputs $T_{\max}$ and $T_{\min}$ were also validated with the corresponding observed Ta values as these two are crucial variables in both the methods (see Fig. 4). $T_{\max}$ and $T_{\min}$ were estimated using advanced statistical methods, as explained in Section III-B.2 for all-sky conditions. As presented in Fig. 4, $T_{\max}$ performed well with a correlation coefficient (*r*) value of 0.845 and root mean square error (RMSE) value of 1.2 °C, whereas for $T_{\min}$ values, *r* value of 0.766 was within the limit, but RMSE value of 4 °C was found to be high with observed $T_{\min}$ values. AET values estimated using the VI-Kv method yielded better values than the TSEB model with *r* and RMSE values of 0.676 and 0.65 mm/day, respectively, for clear sky conditions. For the estimation of AET using the VI-Kv method, estimated ET_0 and Kv values were also

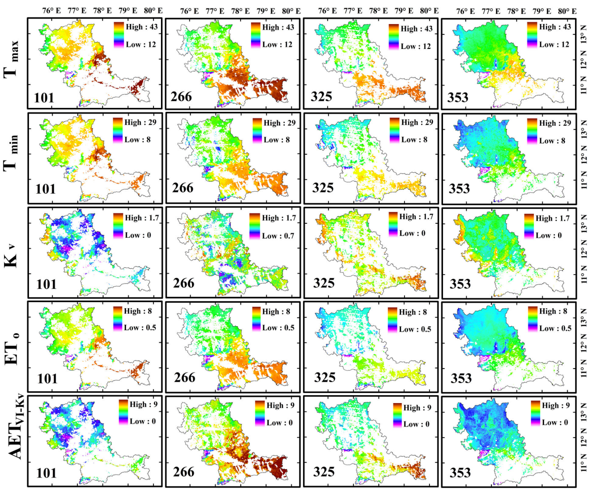

Fig. 5. Spatial variations of $T_{\max}$ (°C), $T_{\min}$ (°C), Kv, ET_0 (mm/day), and ET estimated using the vegetation coefficient method (AET_{VI-Kv}) (mm/day) for 101st, 266th, 325th, and 353th days of the year 2013, representing different seasons for clear pixels.

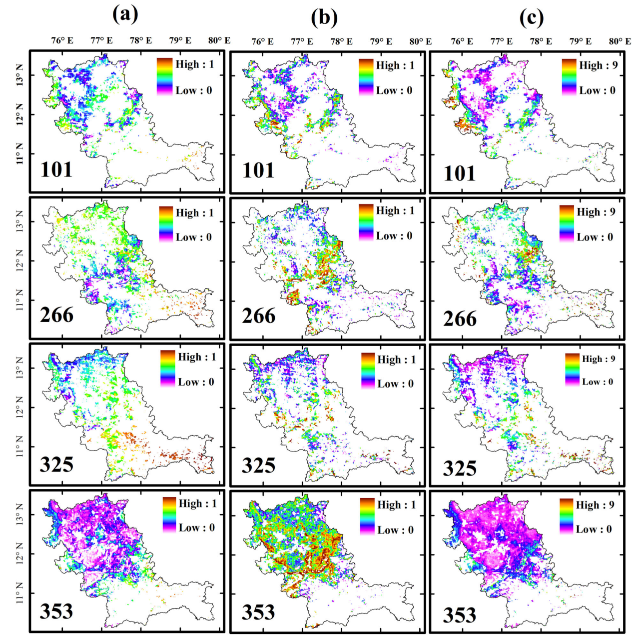

Fig. 6. Spatial variations of EF_{veg} (a), EF_{soil} (b), AET (c) estimated using TSEB methods (mm/day) for 101st, 266th, 325th, and 353th days of the year 2013, representing different seasons for clear pixels.

compared with observed values to check their accuracy. ET_0 was estimated using the PMT_Ta method correlated well with the observed ET_0 with the *r* value of 0.908 and RMSE value of 0.77 mm/day. Estimated Kv values using improved the Kv model gave *r* and RMSE values of 0.722 and 0.21, respectively, with the observed values for clear sky conditions. The TSEB model slightly underestimated daily AET values compared with the VI-Kv method.

The TSEB model provides instantaneous AET values, and these have to be extrapolated to daily values, whereas in the case of the VI-Kv method, such extrapolation is not required as it provides daily AET values directly. In this study, the VI-Kv method has been improved with the inclusion of TVDI along with GVMI to account for both evaporation and transpiration factors [41] and also by selecting the proper temperature-based ET_0 equation [42]. Thermal vegetation index, i.e., TVDI could inherently account for AET reduction due to moisture stress, but this factor was not accounted for in the literature. Therefore, the VI-Kv method gave better AET values than the TSEB model. And also this method requires fewer inputs compared with the TSEB model.

Spatio-temporal variations of $T_{\max}$, $T_{\min}$, ET_0, Kv, and AET estimated using the VI-Kv (AET_{VI-Kv}) method for the days of the year 2013 (101, 266, 325, and 353) representing four seasons, viz., summer, rainy, postmonsoon, and winter, respectively, are illustrated in Fig. 5. Cloudy pixels present in all variables were masked according to the information provided in the quality assessment layer and represented in white color in the study region (see Fig. 5). The cloudy pixels present in all the variables were later filled, details about these filling methods will be provided in coming sections. In summer season, higher $T_{\max}$, $T_{\min}$, and ET_0 and lower Kv and AET_{VI-Kv} values were found over the basin than in other seasons. Western Ghats have higher Kv, ET_0,, and AET_{VI-Kv} values and lower $T_{\max}$ and $T_{\min}$ values than the other parts of the study region since it is covered by forests. Higher AET_{VI-Kv} values were found during rainy and postmonsoon seasons than during the other two seasons. The lower part of the basin has higher $T_{\max}$, $T_{\min}$, ET_0, and AET_{VI-Kv} values than the upper part of the basin. During the rainy season (i.e., 266th day in Fig. 5), lower part of the basin has higher $T_{\max}$ and $T_{\min}$ values than postmonsoon and winter season, because this portion gets rainfall during northwest monsoon, whereas upper part of the basin receives rainfall during the southwest monsoon and hence has lower $T_{\max}$ and $T_{\min}$ values. It was difficult to interpret seasonal changes of these variables in most parts of the basin due to the absence of data during overcast conditions, and these were filled later.

Fig. 6 depicts spatio-temporal variations of AET_{TSEB}, EF_{veg}, and EF_{soil} using the TSEB method for the days of the year 2013 (101, 266, 325, and 353) representing four seasons, viz., summer, rainy, postmonsoon, and winter, respectively. The TSEB model requires a large number of variables, and these were difficult to obtain for most of the pixels of the basin for clear sky condition, and therefore less number of pixels were found compared with AET_{VI-Kv} [see Fig. 6(c)]. The TSEB model underestimated AET values for all the seasons compared with the VI-Kv method. In this case, higher AET values were found in the Western Ghats than other parts of the basin, but these were lesser than AET_{VI-Kv}. In the rainy season, higher AET_{TSEB} was found compared with other seasons. Spatial variations of EF_{veg} and EF_{soil} are also presented in Fig. 6(a) and (b). In rainy and postmonsoon seasons, EF_{veg} values were high compared with other seasons. In contrast to this, EF_{soil} values were low for these two seasons, whereas for summer and winter seasons, EF_{soil} yielded higher values than for the other two seasons, and EF_{veg} showed lower values for the same pixels. Overall for all seasons and pixels, spatial variations of EF_{soil} showed contrary to the spatial variations of EF_{veg}. Due to cloudy conditions, AET values for many pixels were missing, which impedes the

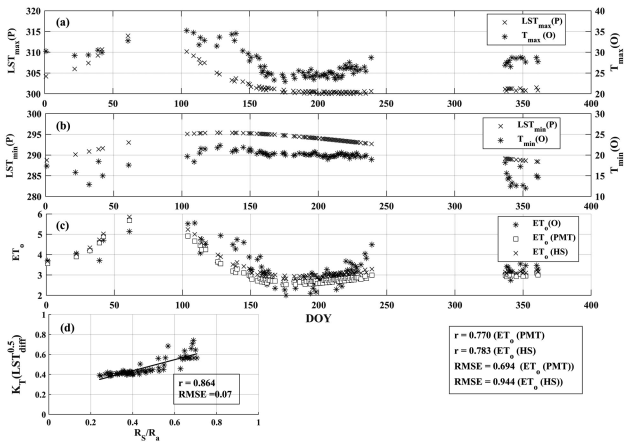

Fig. 7. Comparison of the daily time series of $\mathrm{LST}_{\max}$ (K) (a), $\mathrm{LST}_{\min}$ (K) (b), ET_0 (mm/day) (c) with ground-based measurements of $T_{\max}$ (°C), $T_{\min}$ (°C), and ET_0 at Berambadi station during 2013 under cloudy sky conditions. Observed ET_0 is estimated using FAO56 PM equation from ground-based measurements. Scatter plot between estimated and observed clearness index (d). Missing data are due to gaps in ground measurements.

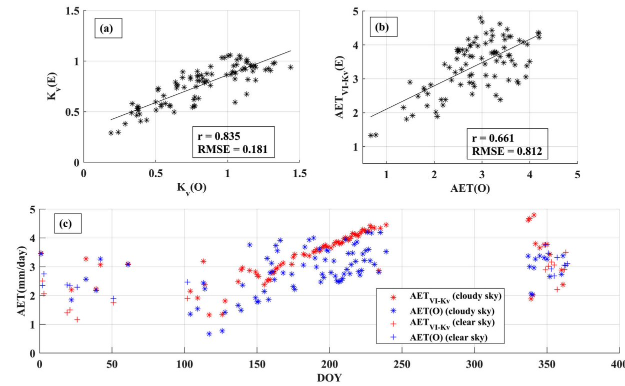

Fig. 8. Scatter plots between $\mathrm{K_v}$ (a), $\mathrm{AET_{VI-Kv}}$ (mm/day) (b) and with their observed values under cloudy sky conditions. Temporal variations of $\mathrm{AET_{VI-Kv}}$ during the year 2013 for all-sky conditions (c). Observed AET values are estimated using Bowen ration technique. Missing data are due to gaps in ground measurements.

application of AET in many fields. Therefore, these pixels were filled using the methodology given in Section III-B.2.

C. Estimation of AET Using Vegetation Coefficient Method for All-Sky Conditions

To determine AET under cloudy sky conditions using the VI-Kv method, required ET_0 was estimated by employing PMT and HS equations and using only LST as inputs. Whereas Kv values under cloudy sky conditions were calculated from the regression technique using Kv values obtained for clear sky conditions [41]. All these variables obtained under cloudy sky conditions were validated with the observed variables of Berambadi station for the year 2013.

Fig. 7 shows that temporal variations of $\mathrm{LST}_{\max}$, $\mathrm{LST}_{\min}$, and ET_0 are obtained from the satellite data, and these were compared with the observed $T_{\max}$, $T_{\min}$, and ET_0 values. Here, observed ET_0 values were calculated using the FAO56-PM equation and observed variables. It can be noticed from Fig. 7(a) and (b) that the differences between $\mathrm{LST}_{\max}$, $\mathrm{LST}_{\min,}$ and $T_{\max}$, $T_{\min}$ were less under cloudy sky conditions and exhibit similar variations. Fig. 7(c) shows that estimated ET_0 using PMT and HS equations were correlated well with the observed ET_0 values. It was found that the PMT equation slightly performed better than HS equations with less RMSE value of 0.694 mm/day. In these two equations, the effect of cloud cover is accounted for by estimation of Rs using (17), where, the difference between the $T_{\max}$ and $T_{\min}$ depends on the degree of cloud cover. On cloudy days, the amount of solar radiation reaching the earth's surface reduces, resulting in reduced $T_{\max}$ during the daytime. On the other hand, at night under cloudy sky conditions, the net outgoing longwave radiation is reduced, thereby raising the $T_{\min}$ compared with clear sky conditions. This effect is shown in Fig. 7(d), which is a scatter plot between $K_T * (\mathrm{LST}_{\max} - \mathrm{LST}_{\min})$ and Rs/Ra (clearness index). The clearness index is estimated using satellite-based $\mathrm{LST}_{\max}$ and $\mathrm{LST}_{\min}$ to obtain the difference, and it is multiplied with K_T, which is on the *y*-axis of the plot. The observed clearness index is obtained from the observed Rs of the Berambadi station and Ra, which is calculated based on the day of the year and latitude. The estimated clearness index compares favorably with the observed clearness index [see Fig. 7(d)], showing less RMSE of 0.07 and a high *r* value of 0.864. This illustrates that $\mathrm{LST}_{\max}$ and $\mathrm{LST}_{\min}$ predicted using MPDI from ANN models are able to capture the effect of clouds, and these two variables are sufficient to estimate ET_0 under cloudy sky conditions.

As a final step, daily AET values were estimated using (11) for cloudy days, and these were evaluated with the observed AET values at Beramabadi station. Fig. 8 describes the relationship between estimated Kv, $\mathrm{AET_{VI-Kv}}$ using satellite data and observed Kv, AET. The proposed methodology yielded better Kv, AET values when compared with the observed values with *r* and RMSE values of 0.835, 0.661 and 0.181, 0.812 mm/day, respectively. This shows that the proposed methodology could fairly estimate $\mathrm{AET_{VI-Kv}}$ values under cloudy sky conditions with limited satellite data. It was also examined how the proposed method captures a general temporal pattern of daily AET for all-sky conditions. Estimated $\mathrm{AET_{VI-Kv}}$ has comparable temporal variation with observed AET [see Fig. 8(c)]. For a few days, the proposed methodology estimated higher AET values than observed values; however, statistical error indices obtained from the available data suggest that the improved methodology (i.e., VI-Kv method) can be successfully applied to estimate daily AET for all-sky conditions.

Spatio-temporal variations of $\mathrm{LST}_{\max}$, $\mathrm{LST}_{\min}$, ET_0, Kv, and $\mathrm{AET_{VI-Kv}}$ for the days of the year 2013 (101, 266, 325, and 353) representing four seasons, viz., summer, rainy, post-monsoon, and winter, respectively, for all-sky conditions are shown in Fig. 9. $\mathrm{LST}_{\max}$ and $\mathrm{LST}_{\min}$ were estimated using day and nighttime AMSR-2 sensor's microwave measurements from ANN models. Western Ghats have lower $\mathrm{LST}_{\max}$ values and higher Kv, ET_0, and $\mathrm{AET_{VI-Kv}}$ values compared with other regions of the study area, since this part of the basin consists of dense forests. Croplands (C) and cropland/natural vegetation (C/NV) dominates the other classes in the basin. During the summer season, $\mathrm{LST}_{\max}$ and $\mathrm{LST}_{\min}$ showed higher values

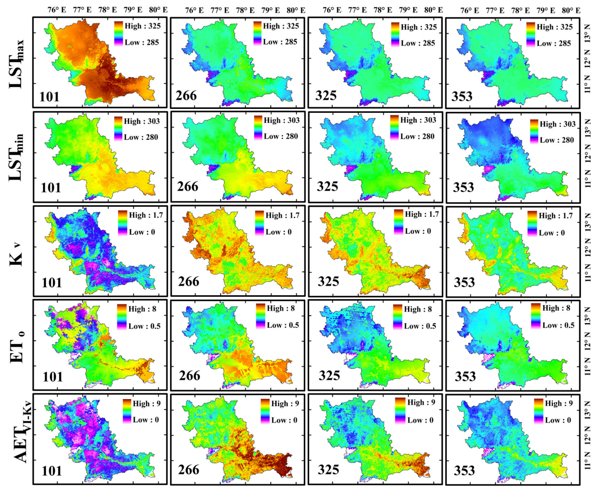

Fig. 9. Spatial variations of $\mathrm{LST}_{\mathrm{max}}$ (K), $\mathrm{LST}_{\mathrm{min}}$ (K), K_v, ET_0 (mm/day), and AET estimated using the vegetation coefficient ($\mathrm{AET}_{\mathrm{VI-Kv}}$) method (mm/day) for 101st, 266th, 325th, and 353th days of the year 2013, representing different seasons for all-sky conditions.

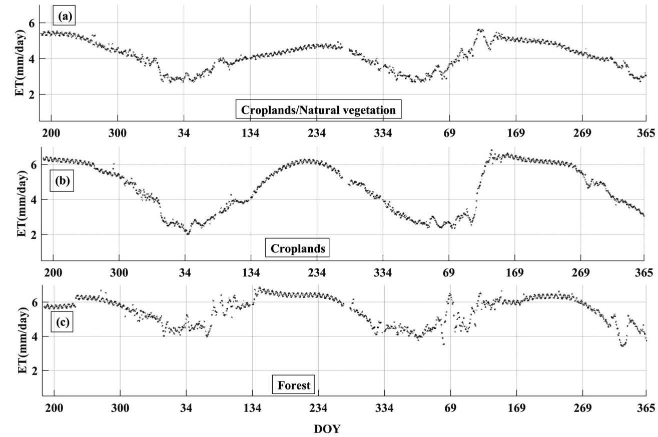

Fig. 10. Temporal variations of AET estimated using vegetation coefficient methods (mm/day) for the years 2012–2014, for croplands/natural vegetation (a), croplands (b), and woody savannas (c) land cover classes of the Cauvery basin for all-sky conditions.

compared with other seasons, whereas Kv and $\mathrm{AET}_{\mathrm{VI-Kv}}$ values were lower compared with other seasons. For these two classes, all the considered variables were found to have lesser values for the cloudy sky conditions compared with clear sky conditions (see Figs. 5 and 9). $\mathrm{LST}_{\mathrm{min}}$ and ET_0 values were higher in the lower part of the basin compared with the upper part of the basin for all seasons, and this is due to lower elevation. Higher $\mathrm{AET}_{\mathrm{VI-Kv}}$ values were observed during rainy and postmonsoon seasons compared with the other two seasons as most agricultural activities take place during this time. Lower $\mathrm{AET}_{\mathrm{VI-Kv}}$ values were seen in the summer season. As a major part of the basin was covered by C or C/NV, estimated ET values for all-sky conditions were validated at Beramadi station as it belongs to C land cover class. Therefore, the proposed methodology can be applied successfully over C or C/NV classes. Furthermore, it is necessary to check the performance of the proposed AET methodology for other land cover classes, especially for forest land. The spatial variations of estimated variables such as ET_0, Kv, and $\mathrm{AET}_{\mathrm{VI-Kv}}$ values, were found to be captured well even for the forest class by visual interpretation. Nevertheless, it will be more beneficial to the AET users, if estimated AET is validated with the observed values for other land cover classes and other climatic conditions.

Temporal variations of AET estimated using the vegetation coefficient method for the years from July 2nd of 2012 (184) to December 30th of 2014 (365) for randomly selected pixels of three AWS stations location [ISRO325_15F145 (IIHR, Hessaraghatta lake post, Bangalore), ISRO387_15F183 (HLBC Subdivision Nagamangala), and ISRO434_15F1B2 (RARS Ambalavayal Wayanad)] representing croplands/natural vegetation, croplands and forest land cover classes for all-sky conditions are shown in Fig. 10. The proposed methodology could even capture the temporal pattern of AET for the study region. It was found that the pixels representing forests have higher AET values compared with the other two land cover classes. Improved vegetation coefficient method could estimate AET values for all-sky conditions with fewer datasets.

V. Conclusion

In this study, daily AET was estimated for all-sky conditions using the VI-Kv method utilizing satellite data. In order to check the potentiality of the VI-Kv method, AET values obtained using this method have been compared with the AET values estimated using widely used and accepted TSEB model for clear sky conditions. Results revealed that the VI-Kv method performed better than the TSEB model. In addition, LST of MODIS cloud product and LST predicted using MPDI with ancillary data were evaluated with in-situ Ta measurements over overcast conditions. It was found that MPDI-based LST correlated well with the Ta for both day and night times. The crucial variable ET_0 was estimated under cloudy sky conditions using predicted $\mathrm{LST}_{\mathrm{max}}$ and $\mathrm{LST}_{\mathrm{min}}$ using MPDI with other ancillary data. These values were multiplied with the Kv values obtained using the regression technique to estimate AET under cloudy sky conditions. Here, only LST values were used to estimate ET_0 under cloudy sky conditions because the predicted $\mathrm{LST}_{\mathrm{max}}$ and $\mathrm{LST}_{\mathrm{min}}$ could capture the variations of ET_0 due to cloud effects, as the difference between $\mathrm{LST}_{\mathrm{max}}$ and $\mathrm{LST}_{\mathrm{min}}$ will be low during cloudy sky conditions and will be high under clear sky conditions. Therefore, this criterion effects the variations of AET under clear and cloudy sky conditions through ET_0 values. This motivated the application of vegetation coefficient method for all-sky conditions. The proposed VI-Kv method could be extended to other regions and other climatic conditions since vital ET_0 and Kv values required in this method could be estimated using available optical and microwave satellite data, as demonstrated in this study. However, the improved Kv model needs to be calibrated before its application in other regions.

It is clearly shown in this study that the proposed VI-Kv method could estimate daily AET for all-sky conditions using only available satellite data. Since reliable and timely estimates of AET are necessary for hydrological and groundwater modeling and water resource planning and to investigate the impacts of climate change on terrestrial systems. However, this method has to be validated with the observed values for different land cover classes other than croplands and under different climatic conditions. Estimation of ET_0 from PMT and HS equations using only LST or Ta values have to be applied carefully for other climatic conditions since these equations are site specific. Future work will be involved with the evaluation of AET_{VI-Kv} values obtained from the improved VI-Kv method with the available AET products.

ACKNOWLEDGMENT

The authors would like to thank Prof. Muddu Shekar (Department of Civil Engg, IISc, Bangalore) and his team for providing observed latent heat flux, solar radiation, and other meteorological data for the Berambadi station. The authors would also like to thank NASA Land Process Distributed Active Archive Center for rendering available MODIS LST, Reflectance, and LULC data and ISRO's MOSDAC for the supply of AWS data.

REFERENCES

[1] G. Fischer, H. Tubiello, V. Veithuizen, and D. Wiberg, "Climate change impacts on irrigation water requirements: Global and regional effects of mitigation," *Technol. Forecasting Social Change*, vol. 74, pp. 1990–2080, 2006.

[2] W. P. Kustas, K. S. Humes, J. M. Norman, and M. S. Moran, "Single and dual source modeling of surface energy fluxes with radiometric temperature." *J. Appl. Meteorol.*, vol. 35, pp. 110–121, 1995.

[3] W. P. Kustas and J. M. Norman, "A two source approach for estimating turbulent fluxes using multiple angle thermal infrared observations," *Water Resour. Res.*, vol. 33, pp. 1495–1508, 1997.

[4] W. P. Kustas and J. M. Norman, "A two source energy balance approach using directional radiometric temperature observations for sparse canopy covered surfaces," *Agronomy J.*, vol. 92, pp. 847–854, 2000.

[5] Z. Su, "The surface energy balance system (SEBS) for estimation of turbulent heat fluxes," *Hydrol. Earth Syst. Sci.*, vol. 6, pp. 85–99, 2002.

[6] C. M. U. Neale, R. K. Vinukollu, and R. D. Ramsey, "A hybrid surface energy balance approach for the estimation of evapotranspiration in agricultural areas," *AIP Conf. Proc.*, vol. 852, pp. 138–145, 2006.

[7] F. Li, W P. Kustas, J. H. Prueger, C. M. U. Neale, and T. J. Jackson, "Utility of remote sensing based two source energy balance model under low and high vegetation cover conditions," *J. Hydrometeorol.*, vol. 6, pp. 878–891, 2005.

[8] R. G. Allen, M. Tasumi, and R. Trezza, "Satellite based energy balance for mapping evapotranspiration with internalized calibration (METRIC)-model," *J. Irrigation Drainage Eng.*, vol. 133, pp. 380–394, 2007.

[9] D. J. Kalma, T. Rm. Mcvicar, and M. F. Mccabe, "Estimating land surface evaporation: A review of methods using remotely sensed surface temperature data," *Surv. Geophys.*, vol. 29, pp. 421–469, 2008.

[10] J. L. Chavez, P. H. Gowda, T. A. Howell, C. M. U. Neale, and K. S. Copeland, "Estimating hourly crop ET using two source energy balance model and multispectral airborne imagery," *Irrigation Sci.*, vol. 28, pp. 79–91, 2009.

[11] R. G. Allen, A. Irmak, R. Trezza, J. M. Hendrickx, W. Bastiaanssen, and J. Kjaersgaard, "Satellite-based ET estimation in agriculture using SEBAL and METRIC," *Hydrol. Processes*, vol. 25, pp. 4011–4027, 2011.

[12] D. Long and V. P. Singh, "A modified surface energy balance algorithm for land (M-SEBAL) based on trapezoidal framework," *Water Resour. Res.*, vol. 48, 2012, Art. no. W02528.

[13] P. D. Colaizzi *et al.*, "Two source energy balance model estimates of evapotranspiration using component and composite surface temperatures," *Adv. Water Resour.*, vol. 50, pp. 134–151, 2012.

[14] R. Guzinski, M. C. Anderson, W. P. Kustas, H. Nieto, and I. Sandhollt, "Using thermal based two source energy balance model with time differencing to estimate surface energy fluxes with day and night MODIS observations," *Hydrol. Earth Syst. Sci.*, vol. 17, pp. 2809–2825, 2013.

[15] W. J. Timmermans, W. P. Kustas, M. C. Anderson, and A. N. French, "An intercomparison of the surface energy balance algorithm for Land (SEBAL) and the two source energy balance (TSEB) modeling schemes," *Remote Sens. Environ.*, vol. 108, pp. 369–384, 2007.

[16] M. Choi, K. William, M. C. Anderson, R. G. Allen, F. Li, and J. H. Kjaersgaard, "An inter comparison of three remote sensing-based surface energy balance algorithms over a corn and soybean production region (Iowa, U.S.) during SMACEX," *Agric. Forest Meteorol.*, vol. 149, no. 12, pp. 2082–2097, 2009.

[17] R. Tang *et al.*, "Evaluating one and two source energy balance models in estimating surface evapotranspiration from Landsat derived surface temperature and field measurements," *Int. J. Remote Sens.*, vol. 34, pp. 1–15, 2013.

[18] J. P. Guerschman *et al.*, "Scaling of potential evapotranspiration with MODIS data reproduces flux observations and catchment water balance observations across Australia," *J. Hydrol.*, vol. 369, pp. 107–119, 2009.

[19] G. P. Edward, P. L. Nagler, and A. R. Huete, "Vegetation index methods for estimating evapotranspiration by remote sensing," *Surv. Geophys.*, vol. 31, pp. 531–555, 2010.

[20] G. P. Edward, C. M. U. Neale, D. J. Hunsaker, and P. L. Nagler, "Vegetation index-based crop coefficients to estimate evapotranspiration by remote sensing in agricultural and natural ecosystems," *Hydrol. Processes*, vol. 25, pp. 4050–4062, 2011.

[21] S. Rossi, A. Rampini, S. Bocchi, and M. Boschetti, "Operational monitoring of daily crop water requirements at the regional scale with time series of satellite data," *J. Irrigation Drainage Eng.*, vol. 136, no. 4, pp. 225–231, 2010.

[22] G. Sun *et al.*, "A general predictive model for estimating monthly ecosystem evapotranspiration," *Ecohydrology*, vol. 4, pp. 245–255, 2011.

[23] H. Nouri, S. Beecham, S. Anderson, A. M. Hassanli, and F. Kazemi, "Remote sensing techniques for predicting evapotranspiration from mixed vegetated surfaces," *Urban Water J.*, vol. 12, no. 5, pp. 380–393, 2015.

[24] M. P. Gonzalez-Dugo *et al.*, "A comparison of operational remote sensing based models for estimating crop evapotranspiration," *Agric. Forest Meteorol.*, vol. 149, pp. 1843–1853, 2009.

[25] J. M. Norman, W. P. Kustas, and K. S. Humes, "A two source approach for estimating soil and vegetation energy fluxes from observations of directional radiometric surface temperature," *Agric. Forest Meteorol.*, vol. 77, pp. 263–293, 1995.

[26] J. M. Norman, W. P. Kustas, J. H. Prueger, and G. R. Diak, "Surface flux estimation using radiometric temperature: A dual temperature difference method to minimize measurement errors," *Water Resour. Res.*, vol. 36, no. 8, pp. 2263–2274, 2000.

[27] S. Consoli and D. Vanella, "Comparisons of satellite based models for estimating evapotranspiration fluxes," *J. Hydrol.*, vol. 513, pp. 475–489, 2014.

[28] T. Luo, A. Jutla, and S. Islam, "Evapotranspiration estimation over agricultural plains using MODIS data for all sky conditions," *Int. J. Remote Sens.*, vol. 36, no. 5, pp. 1235–1252, 2015.

[29] K. Wang, R. E. Dickinson, and S. Liang, "Observational evidence on the 759 effects of clouds and aerosols on net ecosystem exchange and evapotranspiration," *Geophys. Res. Letters*, vol. 35, 2008, L10401, doi: 10.1029/2008GL034167.

[30] M. Tasumi, R. G. Allen, R. Trezza, and J. L. Wright, "Satellite based energy balance to assess within population variance of crop coefficient curves," *J. Irrigation Drainage Eng.*, vol. 131, pp. 94–109, 2005.

[31] R. G. Allen, A. J. Clemmens, C. M. Burt, K. Solomon, and T. O'Halloran, "Prediction accuracy for projectwide evapotranspiration using crop coefficients and reference evapotranspiration," *J. Irrigation Drainage Eng.*, vol. 131, no. 1, pp. 24–36, 2005.

[32] T. G. V. Niel *et al.*," Upscaling latent heat flux for thermal remote sensing studies: Comparison of alternative approaches and correction of bias," *J. Hydrol.*, vol. 468/469, pp. 35–46, 2012.

[33] J. Kim and T. S Hogue, "Evaluation of a MODIS based potential evapotranspiration product at the point scale," *J. Hydrometeorol.*, vol. 9, pp. 444–460, 2007.

[34] Z. Ruan, J. Li, and M. Menenti, "Evaluation of algorithms to estimate daily evapotranspiration from instantaneous measurements under all sky conditions," *IOP Conf. Ser.: Earth Environ. Sci.*, vol. 17, 2014, Art. no. 012133.

[35] W. P. Kustas and J. M. Norman, "Use of remote sensing for evapotranspiration monitoring over land surfaces," *Hydrol. Sci. J.*, vol. 41, no. 4, pp. 495–516, 1996.

[36] J. Sun, G. D. Salvucci, and D. Entekhabi, "Estimates of evapotranspiration from MODIS and AMSR-E land surface temperature and moisture over the Southern Great Plains," *Remote Sens. Environ.*, vol. 127, pp. 44–59, 2012.

[37] W. G. M. Bastiaanssen, M. J. M. Cheema, W. W. Immerzeel, I. J. Miltenburg, and H. Pelgrum, "Surface energy balance and actual evapotranspiration of the transboundary Indus basin estimated from satellite measurements and the ETLook model," *Water Resour. Res.*, vol. 48, pp. 1–16, 2012.
[38] L. Pei, Z-L. Li, Si-Bo. Duan, R. Tang, and M. -. F. Gao, "A method for deriving all-sky evapotranspiration from the synergistic use of remotely sensed images and meteorological data," *J. Geophys. Res., Atmos.*, vol. 122, pp. 13263–13277, 2017.
[39] F. Li, W. P. Kustas, M. C. Anderson, T. J. Jackson, R. Bindlish, and J. H. Prueger, "Comparing utility of microwave and thermal remote sensing constraints in two source energy balance modeling over an agricultural landscape," *Remote Sens. Environ.*, vol. 101, pp. 315–328, 2006.
[40] H. R. Shwetha, and D. N. Kumar, "Prediction of high spatio-temporal resolution of land surface temperature under cloudy sky conditions using microwave vegetation index and ANN," *ISPRS J. Photogramm. Remote Sens.*, vol. 117, pp. 40–55, 2016.
[41] H. R. Shwetha, and D. N. Kumar, "Estimation of daily vegetation coefficients using MODIS data for clear and cloudy sky conditions," *Int. J. Remote Sens.*, vol. 39, no. 11, pp. 3776–3800, 2018.
[42] H. R. Shwetha, and D. N. Kumar, "Performance evaluation of satellite based air temperature and reference evapotranspiration over a river basin," *Hydrol. Sci. J.*, vol. 63, no. 9, pp. 1347–1367, 2018.
[43] CWC and NRSC (Central Water Commission and National Remote Sensing Centre). Cauvery Basin Report. (2014). Accessed Nov. 17, 2016. [Online]. Available: www.india-wris.nrsc.gov.in
[44] J. Dwyer and G. Schmidt, "The MODIS reprojection tool," in *Earth Science Satellite Remote Sensing*, J. J. Qu *et al.*, Eds. Berlin, Germany: Springer, 2006.
[45] M. Sekhar *et al.*, "A manual for agro-hydrological monitoring in pilot experimental watersheds," Indian Institute of Science, Bengaluru, India, 2015.
[46] B. Gautam, and B. L. Rafael, "Estimation of net radiation from the MODIS data under all sky conditions: Southern Great Plains case study," *Remote Sens. Environ.*, vol. 114, pp. 1522–1534, 2010.
[47] K. Gallo, R. Hale, D. Tarpley, and Y. Yu, "Evaluation of relationship between air and land surface temperature under clear and cloudy conditions," *J. Appl. Meteorol. Climatol.*, vol. 50, pp. 767–775, 2011.
[48] J. Catherinot, *et al.*, "Evaluation of "all weather" microwave-derived land surface temperatures with in situ CEOP measurements," *J. Geophys. Res.*, vol. 116, D23105, pp. 1–11, 2011.
[49] K. Nishida, R. R. Nemani, S. W. Running, and J. M. Glassy, "An operational remote sensing algorithm of land surface evaporation," *J. Geophys. Res.*, vol. 108, D9, 4270, pp. 1–14, 2003.
[50] M. Todorovic, B. Karic, and L. Pereira, "Reference evapotranspiration estimate with limited weather data across a range of Mediterranean climates," *J. Hydrol.*, vol. 481, pp. 166–176, 2013.
[51] A. Musy, B. Hingray, and C. Picouet, *Hydrology: A Science for Engineers*. Boca Raton, FL, USA: CRC Press, 2015.
[52] Z. Samani, "Estimating solar radiation and evapotranspiration using minimum climatological data," *J. Irrigation Drainage Eng.*, vol. 126, no. 4, pp. 265–267, 2000.
[53] R. G. Allen, "Evaluation procedures for estimating mean monthly solar radiation from air temperature," United Nations Food and Agricultural Organization (FAO), Rome, Italy, 1995.
[54] G. H. Hargreaves, "Simplified coefficients for estimating monthly solar radiation in North America and Europe," Departmental paper, Dept. Biol. Irrigation Eng., Utah State Univ., Logan, UT, USA, 1994.
[55] M. Smith, "Report on the expert consultation on procedures for revision of FAO guidelines for prediction of crop water requirements," FAO, Rome, Italy, 1991.

Hassan Rangaswamy Shwetha received the B.Tech. degree in civil engineering from the Malnad College of Engineering, Hassan, India, in 2009, M.Tech. degree in remote sensing and GIS from the National Institute of Technology Surathkal, Mangalore, India, in 2011, and Ph.D. degree in civil engineering from the Indian Institute of Science, Bangalore, India, in 2017.

She was a Research Associate with the Interdisciplinary Centre for Water Research, Indian Institute of Science. She is currently an Assistant Professor with the Department of Applied Mechanics and Hydraulics, National Institute of Technology, Surathkal. Her research interests include optical, thermal, and microwave remote sensing, and applications of remote sensing in agricultural hydrology.

Dasika Nagesh Kumar received the Ph.D. degree in civil engineering from the Indian Institute of Science, Bangalore, India, in 1992.

He was a Boyscast Fellow with the Utah Water Research Laboratory, Utah State University, Logan, UT, USA, in 1999. He was with IIT, Kharagpur, India, and National Remote Sensing Centre, Hyderabad, India. He has been a Professor with the Department of Civil Engineering, Indian Institute of Science, Bangalore, India, since May 2002. He has coauthored six textbooks and authored more than 200 papers, including 118 in peer-reviewed journals. His research interests include climate hydrology, climate change, water resource systems, ANN, evolutionary algorithms, fuzzy logic, MCDM, and remote sensing and GIS applications in water resource engineering (http://www.civil.iisc.ac.in/~nagesh).